Journal of Dental Research
2016, Vol. 95(12) 1394–1400

DOI: 10.1177/0022034516662022
jdr.sagepub.com

Silica Coating of Nonsilicate Nanoparticles for Resin-Based Composite Materials

M.R. Kaizer[1], J.R. Almeida[1], A.P.R. Gonçalves[1], Y. Zhang[2], S.S. Cava[3], and R.R. Moraes[1]

Abstract

This study was designed to develop and characterize a silica-coating method for crystalline nonsilicate ceramic nanoparticles (Al_2O_3, TiO_2, and ZrO_2). The hypothesis was that the coated nonsilicate nanoparticles would stably reinforce a polymeric matrix due to effective silanation. Silica coating was applied via a sol-gel method, with tetraethyl orthosilicate as a silica precursor, followed by heat treatment. The chemical and microstructural characteristics of the nanopowders were evaluated before and after silica coating through x-ray diffraction, BET (Brunauer-Emmett-Teller), energy-dispersive x-ray spectroscopy, field emission scanning electron microscopy, and transmission electron microscopy analyses. Coated and noncoated nanoparticles were silanated before preparation of hybrid composites, which contained glass microparticles in addition to the nanoparticles. The composites were mechanically tested in 4-point bending mode after aging (10,000 thermal cycles). Results of all chemical and microstructural analyses confirmed the successful obtaining of silica-coated nanoparticles. Two distinct aspects were observed depending on the type of nanoparticle tested: 1) formation of a silica shell on the surface of the particles and 2) nanoparticle clusters embedded into a silica matrix. The aged hybrid composites formulated with the coated nanoparticles showed improved flexural strength (10% to 30% higher) and work of fracture (35% to 40% higher) as compared with composites formulated with noncoated nanoparticles. The tested hypothesis was confirmed: silanated silica-coated nonsilicate nanoparticles yielded stable reinforcement of dimethacrylate polymeric matrix due to effective silanation. The silica-coating method presented here is a versatile and promising novel strategy for the use of crystalline nonsilicate ceramics as a reinforcing phase of polymeric composite biomaterials.

Keywords: CAD-CAM, microscopy, nanotechnology, polymers, surface properties, silane

Introduction

An important class of biomaterials includes dental polymer-based composites, which are often reinforced by glass microparticles, silica, and/or zirconia (Zr) nanoparticles (Ferracane 2011; Kaizer et al. 2014) or, as more recently shown, porous 3-dimensional ceramic scaffolds infiltrated with polymer (Swain et al. 2015). Polymers with inorganic particles are effectively reinforced by using organosilanes as coupling agents. Silanes act at the interface of the matrix and reinforcing particles, promoting chemical interfacial interaction between phases (Brown 1980; Nishiyama et al. 1991; Mohsen and Craig 1995; Wilson et al. 2005; Wilson and Antonucci 2006; Wilson et al. 2007; Sideridou and Karabela 2009).

In restorative dental applications, an effective and stable silanation is required due to the harsh aging conditions to which polymer-based composites are exposed. This prerequisite restricts the use of nonsilicate ceramic particles, as they are poorly reactive to silanes. To our knowledge, only one current strategy is effectively used in commercial dental materials to overcome this drawback: clustering silica and Zr nanoparticles (Mitra et al. 2003). Although effective, this approach requires chemical interference with Zr crystals during their synthesis, which hinders modification of crystalized powders. In addition, it is a proprietary approach that, since its publication, is still limited to Zr nanoparticles.

Previous studies (Abboud et al. 1997; Guo et al. 2006) showed that a polymeric matrix can be reinforced by nonsilicate ceramic nanoparticles silanated through heat-modified methods. However, the stability of such reinforcing effects was not tested under aging conditions. The investigation would widen with the creation of a versatile method of making each and every type of nonsilicate ceramic particle prone to

[1]Graduate Program in Dentistry, Federal University of Pelotas, Pelotas, Brazil
[2]College of Dentistry, New York University, New York, NY, USA
[3]School of Materials Engineering, Federal University of Pelotas, Pelotas, Brazil

A supplemental appendix to this article is published electronically only at http://jdr.sagepub.com/supplemental.

Corresponding Author:
R.R. Moraes, Graduate Program in Dentistry, Federal University of Pelotas, Rua Gonçalves Chaves 457, Room 505, 96015-560 Pelotas-RS, Brazil.
Email: moraesrr@gmail.com

effective and stable silanation. This would allow modification of dental composites by addition of ceramic particles with varied chemical and physical characteristics. Therefore, this study was designed to develop and characterize a silica-coating method for crystalline nonsilicate ceramic nanoparticles. The present study also tested the hypothesis that the nanoparticles coated by this method would stably reinforce a polymeric matrix due to effective silanation.

Experiment

Materials

Three types of crystalline nonsilicate ceramic nanoparticles were acquired (Nanoamor): gamma aluminum oxide (99.97% Al_2O_3), commercially available as 1020MR; anatase titanium oxide (99% TiO_2), commercially available as 5420HT; and monoclinic zirconium oxide (99% ZrO_2), commercially available as 5931HT. For the silica-coating process, the as-received powders were immersed in a tetraethylorthosilicate (TEOS) solution (Sigma-Aldrich) and heat treated as described below. Therefore, 6 groups were tested: alumina (Al), silica-coated Al (AlSi), titania (Ti), silica-coated Ti (TiSi), Zr, and silica-coated Zr (ZrSi).

Silica-Coating Method

The nanoparticles were coated with a silica layer applied through a sol-gel method. The particles were dispersed in an aqueous solution of 0.1M hydrochloric acid proanalysis (PA). The suspension was kept in vigorous magnetic stirring for 15 min to prevent aggregation by ionization of the particles. According to a pilot study, TEOS was added to the suspension in the proportion of 40 vol% relative to the volume of nanoparticles, thus adjusting the amount of TEOS according to the density of each material. Vigorous magnetic stirring was maintained, and the temperature was raised to 60 °C to evaporate the aqueous content. After drying, the particles were heat treated in an air atmosphere oven with a 5 °C/min heating rate up to 900 °C dwell temperature for 2 h.

Microstructural and Chemical Characterization of the Ceramic Powders

Micromorphology of the coated and noncoated nanoparticles was analyzed by field emission scanning electron microscopy (Merlin; Zeiss) and transmission electron microscopy (TEM; JEM 1400, JEOL). For elemental chemical composition, the nanopowders were analyzed with energy-dispersive x-ray spectroscopy (JSM-6610; JEOL). Crystalline phases and crystal sizes were determined by x-ray diffraction (XRD; XRD-6000, Shimadzu) with CuKα radiation operating at 40 kV and 40 mA, a scan rate of 4°/min, 2θ range from 10° to 80°, and room temperature. The specific surface area and average particle size of the powders were determined with a BET (Brunauer-Emmett-Teller) analyzer (Quantachrome Nova 1000e) by means of N_2 adsorption/desorption isotherm analysis.

Preparation and Characterization of Hybrid Resin Composites

Resin composites with coated or noncoated nanoparticles were prepared, aged, and mechanically tested to verify the study hypothesis. The formulations did not emulate commercial materials but included a controlled internal comparison: composite with coated particles versus composite with noncoated particles. This was chosen to investigate the effect of silica coating on the interfacial bonding between matrix and nanoparticles to its maximum extent within the experimental conditions of the study. The distinct nanoparticles were used for testing the versatility and effectiveness of the silica-coating method with particles having distinct chemical and physical characteristics. The organic phase of the composites contained a dimethacrylate comonomer blend of 50 wt% 2,2-bis[4-(2-hydroxy-3-methacryloyloxypropyl)phenyl]-propane and 50 wt% triethylenoglycol dimethacrylate (Esstech Inc.). The mixture was rendered photosensitive by the addition of 0.4 wt% camphorquinone and 0.8 wt% ethyl 4-(dimethylamino)benzoate (Sigma-Aldrich).

Pilot studies were carried out to investigate the maximum level of nanoparticle loading that would not interfere with polymerization potential. A degree of C=C conversion of ~60% was set as the goal, since it is correlated to adequate mechanical properties (Ferracane et al. 1998). Monomodal (nanoparticles only) and bimodal (nanoparticles + glass microparticles) composites, with various proportions of filler loadings, were tested in the pilot studies. Resin composites with Ti particles were the most challenging due to their opacity and poor light-curing penetration. It was found that a maximum of 10 wt% nanoparticles with 40 wt% glass microparticles resulted in adequate polymerization regardless of the nanoparticle type. The experimental composites were then prepared in a flowable consistency by adding a total 50% mass of fillers (1:4 nanoparticles:microparticles) with a centrifugal mixer (SpeedMixer; FlackTek). Presilanated 0.7-μm glass microparticles (Esstech) were used to prepare the nanohybrid composites. All nanoparticles with and without silica coating were silanated with 10 wt% 3-methacryloxypropyl-trimethoxysilane (Sigma-Aldrich) as described elsewhere (Sideridou and Karabela 2009; Karabela and Sideridou 2011). Figure 1 illustrates the interaction of organosilane molecules with the surfaces of coated and noncoated nanoparticles.

Photoactivation procedures were carried out with a light-emitting diode curing unit (Discus Dental) with irradiance of 1,100 mW/cm^2. The degree of C=C conversion was evaluated with Fourier transform midinfrared spectroscopy (FTIR Prestige-21; Shimadzu). Specimens (n = 5) with 2-mm thickness were used, and the measurements correspond to the C=C conversion at the bottom surface, which was in contact with the FTIR crystal. A 2-mm thickness was chosen because it corresponds to that of the 4-point bending bars and the maximum

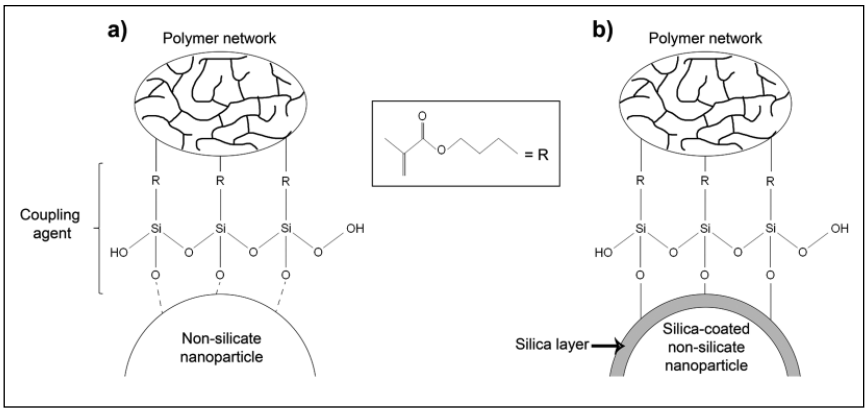

Figure 1. Representative illustration of the interaction among self-assembled crosslinked siloxane layers formed over the nanoparticles modified or not with the silica-coating method. (**a**) The trialkoxysilane function of the organosilane cannot chemically bond to the nanoparticles due to the absence of silica; thus, only physical interactions with the surfaces are formed. A siloxane layer is deposited around the nanoparticles by crosslinking among the silane molecules, but the coupling with the nanoparticle is not effective or stable. (**b**) The presence of a silica layer around the nanoparticles, deposited by the method proposed here, enables effective and stable silanation by formation of siloxane covalent bonds with the now silica-rich surfaces. The methacrylate group on the other end of the organosilane molecules makes the fillers compatible with the polymeric matrix.

polymerization thickness recommended for regular composites.

Bar-shaped specimens (25 × 2 × 2 mm, n = 15) were fabricated for all groups and aged by 10,000 thermal cycles (alternate baths for 30 s in water at 5 ± 5 °C and 55 ± 5 °C). This protocol has been effectively used to stress the filler-matrix interfaces in resin composites (Yoshida et al. 2002). Thermal cycling was chosen since it is a nondestructive aging method. Mechanical fatigue is also often used to age resin composites, but it promotes not only the desired stresses at the filler-matrix interface but also wear, deformation, and cracking, due to cyclic contact (Shembish et al. 2016). Therefore, it would hinder the flexural test intended to be performed after aging.

These specimens were tested in 4-point bending mode (20-mm span length) in a mechanical testing machine (model 5566; Instron) at a crosshead speed of 0.5 mm/min. No preexisting defects were introduced to the bars. Flexural strength (σ_f), flexural modulus (E_f), and work of fracture (WoF) were calculated according to the load-deformation curves (Zhang and Xu 2005; López-Suevos and Dickens 2008; Rodrigues et al. 2008), according to equations 1 to 3:

$$\sigma_f = P_{max}\ L / b\ h^2, \quad (1)$$

$$E_f = (P / d)\ (L^3 / [4\ b\ h^3]), \text{ and} \quad (2)$$

$$WoF = A / b\ h, \quad (3)$$

where P_{max} is the maximum load (N), L the distance between the supports, b the specimen width, and h the specimen height. In equation 2, the load (P) is divided by the corresponding displacement (d) in the linear elastic region of the load-displacement curve. In equation 3, the total area under the load-displacement curve was integrated for calculation.

Results and Discussion

Table 1 shows the results for the elemental composition, particle size, specific surface area, crystal size, and crystalline phases of all particles. The energy-dispersive x-ray spectroscopy elemental analysis showed only the presence of silicon for powders subjected to silica coating. This was corroborated by the presence of quartz in silica-coated particles (XRD analysis). It was noticed that the higher specific surface area of the as-received powders (Al > Ti > Zr) was associated with a higher percentage of silicon after silica coating. Nanoparticles have a significant proportion of atoms on their surfaces. The smaller the particles, the more pronounced the quantum effect on them (Paulus et al. 2001; Scholl et al. 2012). The quantum effect or quantum confinement of nanoparticles makes them susceptible to distinct surface interactions, ranging from simple agglomeration within the powder particles to adsorption of other substances to which they are exposed (Paulus et al. 2001; Scholl et al. 2012).

The particle size analysis before the silica coating showed that all 3 powders were <100 nm, with Al being the smallest particles. The BET diameter increased after silica coating, although only TiSi particles were >100 nm (i.e., outside the nanometer range). This finding indicates a much greater increase in particle size for Ti under the conditions of the silica-coating method described here. It was also observed that the crystal size of Ti particles increased after silica coating, whereas the same did not happen for Al or Zr. It may be assumed that the increase in particle size for AlSi and ZrSi was due to the silica shell present around the particles and not crystal growth or phase transformation (Cava et al. 2007; Isfahani et al. 2014). This is corroborated by the XRD results (Appendix Fig.), which show gamma Al and monoclinic Zr spectra before and after silica coating. Distinctively, Ti spectra differ after silica coating, showing anatase for noncoated powder and anatase + rutile peaks after silica coating. Note that no silica peaks were noticed and that a fraction of only 0.1% quartz phase was estimated, which suggests that the silica layer deposited by the method described herein is amorphous.

TEM images of the nanopowders (Fig. 2) indicated the presence of a silica shell around Zr and Al particles. In Figure 2a (white arrows), it is possible to observe a Zr nanoparticle (darker area at the center) surrounded by a silica layer (grayish area). The thickness of the silica layer seems to vary according to the diameter of the Zr particles, which is evident in the comparison between the 2 examples in Figure 2a (white arrows).

Table 1. Characterizations of the Ceramic Powders: Elemental Composition (EDS), Particle Size and Specific Surface Area (BET), Crystal Size, and Crystalline Phases (XRD).

	EDS, wt.%			EDS, atom%						
	O	Content[a]	Si	O	Content[a]	Si	Surface Area, m^2/g	Particle Size, nm	Crystal Size, nm	Crystalline Phases, %
Al	15.7	84.3	—	24.0	76.0	—	193.2	8.4	4.7	Gamma 100
AlSi	10.7	83.6	5.7	16.9	78.0	5.1	91.1	17.8	5.2	Gamma 99.99 + quartz 0.1
Ti	12.9	87.1	—	30.7	69.3	—	91.9	16.7	25.1	Anatase 100
TiSi	5.4	92.0	2.6	14.5	81.7	3.9	7.3	209.5	88.5	Anatase 97.2 + rutile 2.7 + quartz 0.1
Zr	2.1	98.0	—	10.8	89.2	—	27.3	37.3	32.9	Monoclinic 100
ZrSi	2.4	96.5	1.1	12.1	84.9	3.1	12.5	81.2	36.2	Monoclinic 99.99 + quartz 0.1

BET, Brunauer-Emmett-Teller; EDS, energy-dispersive X-ray spectroscopy; XRD, x-ray diffraction.
Composites: Al, alumina; AlSi, silica-coated Al; Ti, titania; TiSi, silica-coated Ti; Zr, zirconia; ZrSi, silica-coated Zr.
[a]Content of Al, Ti, or Zr according to the powder under evaluation.

Visual particle sizes corroborate the findings of BET and XRD analyses, with AlSi particles (Fig. 2b) being much smaller than ZrSi (Fig. 2a) and TiSi (Fig. 2c) particles. In contrast, the coating method yielded a substantial increase in Ti particle size, which may be attributed to crystal growth and phase transformation during coating (Zhang et al. 2006). XRD analyses of the Ti nanopowders with and without silica coating are also evidence that the increase in particle size is a result of crystal growth and phase transformation (anatase to rutile). TEM images further indicate that the increased BET diameter is explained not only by crystal growth and phase transformation but also by clustering of Ti particles embedded in a silica matrix (hollow black arrows in Fig. 2c), while some discrete coated particles are also present (green arrows). The clusters appear to be ~200 nm in diameter, which is in line with the BET diameter measured for TiSi. All nanoparticles used in this study besides TiSi have a narrow particle size distribution, within the nanometer range even after silica coating (data not shown here). TiSi has a broader distribution due to the presence of discrete nanoparticles and larger nanoclusters. A broad particle size distribution could influence resin/particle packing if maximum nanoparticle loading was used, which was not the case here.

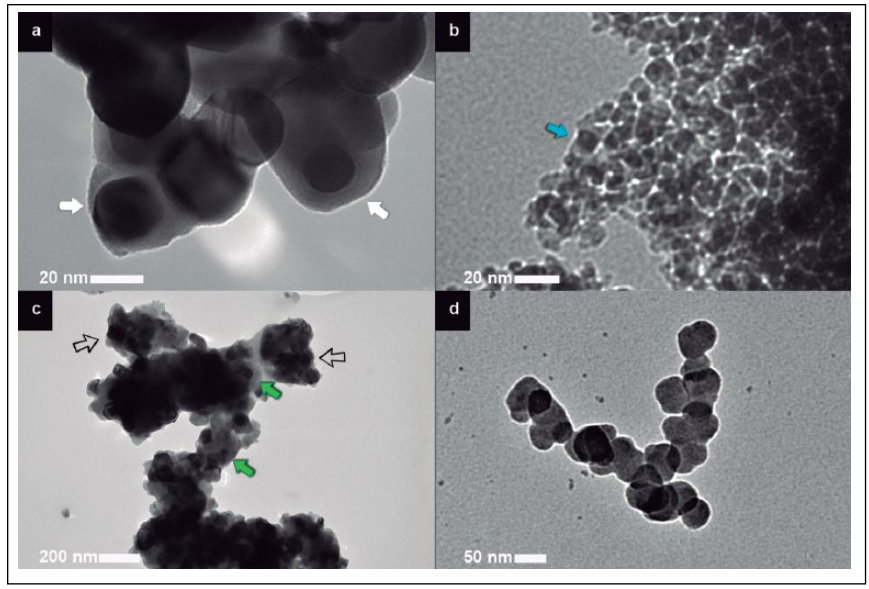

Figure 2. Transmission electron microscopy images of the nanopowders: (**a**) Silica-coated zirconia particles (×1.2M magnification). The white arrows point to zirconia nanoparticles (darker area at the center) surrounded by a silica layer (grayish area). The thickness of the silica layer seems to vary according to the diameter of the zirconia particles, which is visible when the 2 examples indicated by the white arrows are compared. (**b**) Silica-coated alumina particles (×1M magnification). Discrete nanoparticles much smaller than the other particles are observed. The blue arrow points to an example of a coated particle. (**c**) Silica-coated titania particles (×100k magnification). Most particles are seen embedded into clusters with a silica matrix (hollow black arrows), though some coated particles are also present (green arrows). (**d**) Silica nanoparticles (×300k magnification) were detected, most likely as a result of a secondary phase formation during heat treatment of tetraethylorthosilicate molecules that were not bound to the nanopowders in the solution used for the silica-coating method. This figure is available in color online at http://jdr.sagepub.com.

Successful silica coating was demonstrated in this study through 3 types of nonsilicate ceramic nanoparticles with distinct chemical and physical characteristics. The method presented makes the particles prone to effective silanation and thus suitable to be used for a stable reinforcement of a polymer matrix (Brown 1980; Nishiyama et al. 1991; Mohsen and Craig 1995; Wilson et al. 2005; Wilson and Antonucci 2006; Wilson et al. 2007; Sideridou and Karabela 2009). The reaction of silane coupling agents with silica-rich surfaces involves hydrolysis of the silane alkoxy groups into silanol groups, followed by condensation into oligomers that hydrogen bond with hydroxyl groups present at the particle surface. As the silane

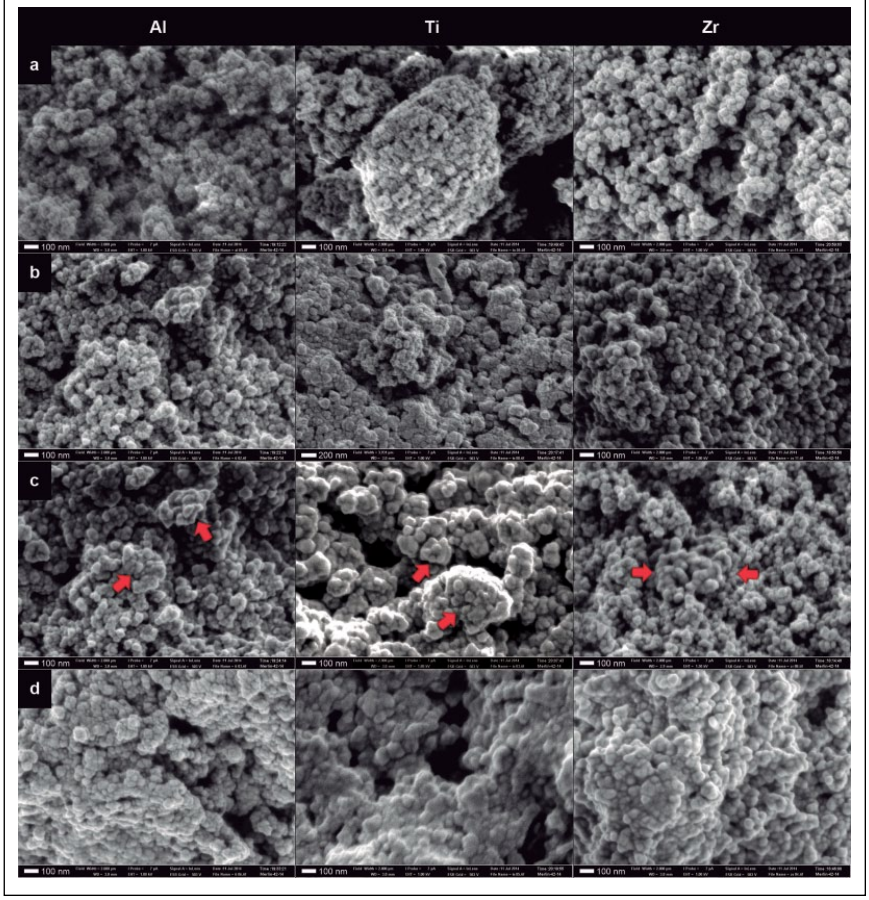

Figure 3. Field emission scanning electron microscopy images of the nanopowders. Imaging conditions: electron beam set at 1 kV and 7 pA, sample distance 3 mm, and imaged in a field width of 2 µm—equivalent to approximately ×180k magnification: (**a**) Image of the nanopowders as received. Alumina (Al) particles are visibly smaller than the other particles. (**b**) Image of the nanopowders after silica coating. Most of the titania (Ti) particles are embedded into clusters with a silica matrix, which does not seem to happen with the other particles. All particles became highly unstable after silica coating (**c**), where some areas in the field (red arrows) show the particles fused as a reaction to the energy of the microscope beam. This is clearly seen for the silica-coated zirconia image, where the fusing started near the reduced focus area in the center of the field. (**d**) The uncontrolled fusing of particles, caused by the energy of the beam and taking over the entire field, thereby generating a 3-dimensional porous structure. This figure is available in color online at http://jdr.sagepub.com.

dries and water is lost, covalent siloxane bonds are formed and improve the resin-filler interfacial strength. The TEM analysis also indicated the presence of silica nanoparticles (Fig. 2d), most likely a result of a secondary phase formation during heat treatment of TEOS molecules that were not bound to the crystalline particles in the solution. Those particles are naturally reactive to silanes; thus, there is no expectation of a negative effect from their presence.

Field emission scanning electron microscopy images of the nanopowders are presented in Figure 3. The analysis reinforces that the Al group has the smallest particles (Fig. 3a). Most of the TiSi particles are embedded into clusters with a silica matrix, which does not seem to happen with the other particles (Fig. 3b), thereby corroborating the findings of the TEM analysis. The silica-coated particles of the 3 groups became highly sensitive to the energy of the microscope, presenting fusing and apparent particle growth. These changes happened progressively with scanning time. The images presented in Figure 3b were taken with a shorter scanning time to preserve particle features. The effects of the instability of the particles are shown in Figure 3c and are represented by the areas in the field showing fused particles (red arrows). Figure 3c for ZrSi particles clearly indicates that this fusing is an effect of the heat generated by the electron collision of the microscope beam: fusing happened only at the center of the field, where the beam scanned for a longer time during image focusing. The whole field was scanned at once during image capture, and that is why the particles around the fused area have their features preserved. In addition, Figure 3d shows the uncontrolled fusing of particles caused by continuous exposure to the beam energy, taking over the entire field and generating a 3-dimensional porous structure. The formation of these porous structures was not the primary aim of the silica-coating method. However, those scaffolds could function as 3-dimensional network preforms for polymer infiltration and preparation of double-network composite blocks for CAD-CAM. Polymer-based composites with interpenetrating phases, which are characterized by porous 3-dimensional ceramic scaffolds infiltrated by a polymer matrix, have recently drawn attention in the literature and shown promising results (He and Swain 2011; Coldea et al. 2013; Nguyen et al. 2013; Coldea et al. 2014; Della Bona et al. 2014; Nguyen et al. 2014; Okada et al. 2014; Coldea et al. 2015). However, the use of crystalline non-silicate particles has not yet been tested for the development of such materials.

Characterizations of the experimental hybrid composites containing the nanoparticles are presented in Table 2. All materials achieved an adequate degree of C=C conversion. Before mechanical testing, the specimens were subjected to 10,000 thermal cycles. Thermal cycling produces degradation through thermally induced interfacial stresses due to a high thermal gradient between filler particles and the resin matrix (Montes and Draughn 1986). These stresses may lead to gap formation or bond strength degradation at the filler-resin interface, thereby compromising the fracture resistance of the composite (Montes and Draughn 1986; Yoshida et al. 2002). The composites prepared with silica-coated nanoparticles presented significantly higher σ_f (10% to 30% higher) and WoF (35% to 40% higher) than their counterparts without silica coating,

Table 2. Flexural Strength, Flexural Modulus, Work of Fracture, and Degree of C=C Conversion of All Hybrid Resin Composites Tested.

Composite	σ_f, MPa	E_f, GPa	WoF, kJ.m$^{1/2}$	DC, %
Al	57.9 (9.1)[b]	7.3 (1.0)	1.4 (0.4)[b]	62.0 (1.6)
AlSi	63.9 (5.7)[a]	7.0 (1.2)	1.9 (0.5)[a]	67.4 (1.1)
Ti	53.1 (7.1)[b]	6.7 (1.1)	1.4 (0.3)[b]	54.0 (1.1)
TiSi	63.4 (6.9)[a]	6.5 (1.7)	1.9 (0.5)[a]	54.9 (1.1)
Zr	52.0 (8.1)[b]	5.2 (1.6)	1.7 (0.7)[b]	62.3 (1.9)
ZrSi	70.3 (6.4)[a]	6.1 (2.0)	2.4 (0.4)[a]	62.4 (1.9)

Values presented as means (SD). σ_f, E_f, and WoF were measured after 10,000 thermal cycles. Distinct letters indicate statistical differences between groups with and without silica coating within the same type of particle (5%).
Mechanical testing: σ_f, flexural strength; DC, degree of C=C conversion; E_f, flexural modulus; WoF, work of fracture. Composites: Al, alumina; AlSi, silica-coated Al; Ti, titania; TiSi, silica-coated Ti; Zr, zirconia; ZrSi, silica-coated Zr.

whereas E_f was not affected by silica coating. E_f was calculated per the elastic portion of the load-deformation curve, where bending of the specimens is not yet sufficient to show differences between groups with coated and noncoated particles. Similar findings were reported when composite materials with silanation of the filler particles were compared with those without silanation (Kinloch et al. 1985; Guo et al. 2006). σ_f and WoF are measured by the elastic and plastic portions of the load-deformation curve. When plastic deformation takes place through the polymeric matrix and blunts the tip of a growing crack (Kinloch et al. 1985), the polymer-particle interface is subjected to tensile stresses (Broutman and Agarwal 1974; Khaund et al. 1977). In such a situation, poor interfacial interaction between the polymeric matrix and fillers results in gap formation and facilitates fracture (Kinloch et al. 1985). The increased resin-filler interfacial strength allowed by silica coating improves mechanical performance by leading to better load transfer and toughening. The results observed herein are therefore associated with a stable chemical bond between the silica layer and silane molecules, which yielded a strong interfacial bond between the polymer matrix and filler particles, ultimately resulting in higher fracture resistance. For the noncoated particles, the lack of silica leads to the formation of weaker interactions between silane molecules and filler surfaces, as opposed to the strong covalent siloxane bonds formed when the silica coating is present (Fig. 1).

The hybrid resin composites tested in the present study had only 10 wt% nanoparticles, while 40 wt% of fillers were composed by silanated glass microparticles. Despite the relatively low fraction of nanoparticles, significant differences were already observed between groups with coated and noncoated particles. The improved silanation obtained through the method shown here could yield even more pronounced mechanical effects if higher nanoparticle fractions were used. Tensile stress fields around particles (Broutman and Agarwal 1974; Khaund et al. 1977) interact due to their proximity in highly filled composites, and gap formation between matrix and particles is more likely to occur if the interfacial interaction is poor. Note that higher filler loading and higher percentages of nanoparticles, even preparation of monomodal nanofilled composites, are still feasible. However, it would be necessary to calculate the ideal nanoparticle size by means of the Rayleigh scattering model to model translucency and the degree of C=C conversion (Jillavenkatesa et al. 2001; Cox et al. 2002; Zhang 2014). In addition, since mechanical fatigue is the most relevant aging method to predict the clinical performance of dental restoratives, it should be investigated in future studies with experimental materials and commercial composites. In that scenario, a potential improvement in the properties of composites obtained through the strategy proposed here as compared with commercial formulations can be investigated.

Conclusion

Successful silica coating was demonstrated through 3 types of nonsilicate nanoparticles with distinct chemical and physical characteristics. Two distinct aspects, depending on the type of coated nanoparticle, were observed: 1) formation of a silica shell on the surface of the nanoparticles and 2) formation of nanoparticle clusters embedded into a silica matrix. Hybrid resin composites reinforced by silica-coated nanoparticles showed improved mechanical performance after aging as compared with the noncoated counterparts. The method might be considered a promising novel strategy for the use of crystalline nonsilicate fillers in dental composites.

Author Contributions

M.R. Kaizer, contributed to conception, design, data acquisition, analysis, and interpretation, drafted and critically revised the manuscript; J.R. Almeida and A.P.R. Gonçalves, contributed to conception and data acquisition, drafted and critically revised the manuscript; Y. Zhang, S.S. Cava, and R.R. Moraes, contributed to conception, design, data acquisition, analysis, and interpretations, drafted and critically revised the manuscript. All authors gave final approval and agree to be accountable for all aspects of the work.

Acknowledgments

The study was supported by CNPq (Conselho Nacional de Desenvolvimento Científico e Tecnológico, Brazil: 141129/2011-5 [PhD scholarship, GD], 241021/2012-0 [PhD internship abroad, SWE], 475462/2012-2 [grant, CNPq Universal]), the National Institutes of Health / National Institute of Dental and Craniofacial Research (2R01 DE017925), and the Department of Chemistry at New York University. The Zeiss Merlin field emission scanning electron microscopy was acquired through the support of the National Science Foundation (DMR-0923251). The authors thank

CEME-Sul (Centro de Microscopia Eletrônica da Zona Sul at Federal University of Rio Grande, Brazil) for transmission electron microscopy support, IQ-USP (Instituto de Química at University of São Paulo, Brazil) for BET analysis, and Esstech Inc. for donation of reagents used in the study. The authors declare no potential conflicts of interest with respect to the authorship and/or publication of this article.

References

Abboud M, Turner M, Duguet E, Fontanille M. 1997. PMMA-based composite materials with reactive ceramic fillers: 1. Chemical modification and characterisation of ceramic particles. J Mater Chem. 7(8):1527–1532.

Broutman LJ, Agarwal BD. 1974. Theoretical study of effect of an interfacial layer on properties of composites. Polym Eng Sci. 14(8):581–588.

Brown SK. 1980. Mechanisms of fracture in filled thermosetting resins. Brit Polym J. 12(1):24–30.

Cava S, Tebcherani SM, Souza IA, Pianaro SA, Paskocimas CA, Longo E, Varela JA. 2007. Structural characterization of phase transition of Al2O3 nanopowders obtained by polymeric precursor method. Mater Chem Phys. 103(2–3):394–399.

Coldea A, Fischer J, Swain MV, Thiel N. 2015. Damage tolerance of indirect restorative materials (including PICN) after simulated bur adjustments. Dent Mater. 31(6):684–694.

Coldea A, Swain MV, Thiel N. 2013. Mechanical properties of polymer-infiltrated-ceramic-network materials. Dent Mater. 29(4):419–426.

Coldea A, Swain MV, Thiel N. 2014. Hertzian contact response and damage tolerance of dental ceramics. J Mech Behav Biomed Mater. 34:124–133.

Cox AJ, DeWeerd AJ, Linden J. 2002. An experiment to measure Mie and Rayleigh total scattering cross sections. Am J Phys. 70(6):620–625.

Della Bona A, Corazza PH, Zhang Y. 2014. Characterization of a polymer-infiltrated ceramic-network material. Dent Mater. 30(5):564–569.

Ferracane JL. 2011. Resin composite—state of the art. Dent Mater. 27(1):29–38.

Ferracane JL, Berge HX, Condon JR. 1998. In vitro aging of dental composites in water—effect of degree of conversion, filler volume, and filler/matrix coupling. J Biomed Mater Res. 42(3):465–472.

Guo ZH, Pereira T, Choi O, Wang Y, Hahn HT. 2006. Surface functionalized alumina nanoparticle filled polymeric nanocomposites with enhanced mechanical properties. J Mater Chem. 16(27):2800–2808.

He LH, Swain M. 2011. A novel polymer infiltrated ceramic dental material. Dent Mater. 27(6):527–534.

Isfahani TD, Javadpour J, Khavandi A, Goodarzi M, Rezaie HR. 2014. Nanocrystalline growth activation energy of zirconia polymorphs synthesized by mechanochemical technique. J Mater Sci Technol. 30(4):387–393.

Jillavenkatesa A, Dapkunas SJ, Lum L. 2001. Particle size characterization. Washington (DC): National Institute of Standards and Technology. Special publication 960-1.

Kaizer MR, de Oliveira-Ogliari A, Cenci MS, Opdam NJ, Moraes RR. 2014. Do nanofill or submicron composites show improved smoothness and gloss? A systematic review of in vitro studies. Dent Mater. 30(4):e41–e78.

Karabela MM, Sideridou ID. 2011. Synthesis and study of properties of dental resin composites with different nanosilica particles size. Dent Mater. 27(8):825–835.

Khaund AK, Krstic VD, Nicholson PS. 1977. Influence of elastic and thermal mismatch on local crack-driving force in brittle composites. J Mater Sci. 12(11):2269–2273.

Kinloch AJ, Maxwell DL, Young RJ. 1985. The fracture of hybrid-particulate composites. J Mater Sci. 20(11):4169–4184.

López-Suevos F, Dickens SH. 2008. Degree of cure and fracture properties of experimental acid-resin modified composites under wet and dry conditions. Dent Mater. 24(6):778–785.

Mitra SB, Wu D, Holmes BN. 2003. An application of nanotechnology in advanced dental materials. J Am Dent Assoc. 134(10):1382–1390.

Mohsen NM, Craig RG. 1995. Effect of silanation of fillers on their dispersability by monomer systems. J Oral Rehabil. 22(3):183–189.

Montes GM, Draughn RA. 1986. In vitro surface degradation of composites by water and thermal cycling. Dent Mater. 2(5):193–197.

Nguyen JF, Migonney V, Ruse ND, Sadoun M. 2013. Properties of experimental urethane dimethacrylate-based dental resin composite blocks obtained via thermo-polymerization under high pressure. Dent Mater. 29(5):535–541.

Nguyen JF, Ruse D, Phan AC, Sadoun MJ. 2014. High-temperature-pressure polymerized resin-infiltrated ceramic networks. J Dent Res. 93(1):62–67.

Nishiyama N, Ishizaki T, Horie K, Tomari M, Someya M. 1991. Novel polyfunctional silanes for improved hydrolytic stability at the polymer-silica interface. J Biomed Mater Res. 25(2):213–221.

Okada K, Kameya T, Ishino H, Hayakawa T. 2014. A novel technique for preparing dental CAD/CAM composite resin blocks using the filler press and monomer infiltration method. Dent Mater J. 33(2):203–209.

Paulus PM, Goossens A, Thiel RC, van der Kraan AM, Schmid G, de Jongh LJ. 2001. Surface and quantum-size effects in Pt and Au nanoparticles probed by Au-197 Mossbauer spectroscopy. Phys Rev B. 64(20):205418.

Rodrigues SA Jr, Ferracane JL, Della Bona A. 2008. Flexural strength and Weibull analysis of a microhybrid and a nanofill composite evaluated by 3- and 4-point bending tests. Dent Mater. 24(3):426–431.

Scholl JA, Koh AL, Dionne JA. 2012. Quantum plasmon resonances of individual metallic nanoparticles. Nature. 483(7390):421–427.

Shembish FA, Tong H, Kaizer M, Janal MN, Thompson VP, Opdam NJ, Zhang Y. 2016. Fatigue resistance of CAD/CAM resin composite molar crowns. Dent Mater. 32(4):499–509.

Sideridou ID, Karabela MM. 2009. Effect of the amount of 3-methacyloxypropyltrimethoxysilane coupling agent on physical properties of dental resin nanocomposites. Dent Mater. 25(11):1315–1324.

Swain MV, Coldea A, Bilkhair A, Guess PC. 2015. Interpenetrating network ceramic-resin composite dental restorative materials. Dent Mater. 32(1):34–42.

Wilson KS, Allen AJ, Washburn NR, Antonucci JM. 2007. Interphase effects in dental nanocomposites investigated by small-angle neutron scattering. J Biomed Mater Res A. 81(1):113–123.

Wilson KS, Antonucci JM. 2006. Interphase structure-property relationships in thermoset dimethacrylate nanocomposites. Dent Mater. 22(11):995–1001.

Wilson KS, Zhang K, Antonucci JM. 2005. Systematic variation of interfacial phase reactivity in dental nanocomposites. Biomaterials. 26(25):5095–5103.

Yoshida Y, Shirai K, Nakayama Y, Itoh M, Okazaki M, Shintani H, Inoue S, Lambrechts P, Vanherle G, Van Meerbeek B. 2002. Improved filler-matrix coupling in resin composites. J Dent Res. 81(4):270–273.

Zhang J, Li MJ, Feng ZC, Chen J, Li C. 2006. UV Raman spectroscopic study on TiO2: I. Phase transformation at the surface and in the bulk. J Phys Chem B. 110(2):927–935.

Zhang Y. 2014. Making yttria-stabilized tetragonal zirconia translucent. Dent Mater. 30(10):1195–1203.

Zhang Y, Xu HH. 2005. Effects of synergistic reinforcement and absorbable fiber strength on hydroxyapatite bone cement. J Biomed Mater Res A. 75(4):832–840.